Journal of Solid State Electrochemistry
https://doi.org/10.1007/s10008-021-04986-y

ORIGINAL PAPER

Structural and electrochemical characterization of vanadium-excess $Li_3V_2(PO_4)_3$-$LiVOPO_4$/C composite cathode material synthesized by sol–gel method

Zishan Ahsan[1] · Zhenfei Cai[1] · Shuai Wang[1] · Yangzhou Ma[1] · Guangsheng Song[1] · Mo Yu[1] · Shihong Zhang[1] · Weidong Yang[2] · Cuie Wen[3] · Xiaohua Feng[4]

Received: 3 February 2021 / Revised: 10 May 2021 / Accepted: 31 May 2021

Abstract

To improve capacity and electrochemical performance of the cathode of Li-ion batteries, non-stoichiometric, vanadium-excess (V-excess) $Li_3V_2(PO_4)_3$-$LiVOPO_4$/C (LVP-LVOP/C) composite cathode materials are synthesized by a single-step citric acid assisted sol–gel method and sintered at temperatures (300–900 °C). X-ray diffraction and transmission electron microscope results indicate that major $Li_3V_2(PO_4)_3$ and minor $LiVOPO_4$ phases coexist and X-ray photoelectron spectroscopy results also show that the valance state of vanadium is + 4 and + 3. The sample sintered at 800 °C shows the best electrochemical performance with the highest discharge capacity of 140 mAh g^{-1} at 0.2 C, higher than the theoretical capacity of $Li_3V_2(PO_4)_3$ in the voltage range 2.8–4.3 V. The composite material displays remarkably improved stability exhibiting reversible capacity of 130, 115, and 108 mAh g^{-1} after 300, 500, and 1000 cycles at the rate of 0.3 C, 0.5 C, and 1 C, respectively. Additionally, the composite LVP-LVOP/C shows superior rate performance at various current densities from 0.2 to 10 C. Our study reveals that the novel composite material considerably enhances electrochemical performance, electronic conductivity, Li-ion diffusion, and contribution of $LiVOPO_4$ to capacity by accommodating extra Li-ions to enhance capacity. The results demonstrate that the study is highly promising for the development of V-excess cathodes as V-excess composite materials exhibit better performance than pure phase $Li_3V_2(PO_4)_3$.

Keywords Dual phase · Vanadium excess · Cathode material · LVP-LVOP/C

✉ Yangzhou Ma
yangzhou.ma@outlook.com

✉ Guangsheng Song
song_ahut@163.com

Zishan Ahsan
zishanahsan87@yahoo.com

1 Key Laboratory of Green Fabrication and Surface Technology of Advanced Metal Materials, Ministry of Education, School of Materials Science and Engineering, Anhui University of Technology, Maanshan 243000, China

2 Future Manufacturing Flagship, Commonwealth Scientific and Industry Research Organization, Melbourne, VIC 3168, Australia

3 School of Engineering, RMIT University, Bundoora, VIC 3083, Australia

4 Key Laboratory of Marine Materials and Related Technologies, Zhejiang Key Laboratory of Marine Materials and Protective Technologies, Ningbo Institute of Materials Technology and Engineering, Chinese Academy of Sciences, Ningbo 315201, China

Introduction

The fast and efficient energy storages are the main requirements in future energy storage devices for the portable (electric vehicles (EVs)) and stationary (solar and wind grid storage) applications [1, 2]. For this purpose, the Li-ion battery (LIB) requires electrode materials with high energy and power density. Especially, cathode materials have gained significant attention as they affect battery's capacity, cycling life, safety, and cost as well [3]. Despite their higher potential, these are limited in capacity compared to anode materials. Currently, lithium metal oxides are being employed for most applications [4]. However, these suffer from the disadvantages of high cost, toxicity, and liberation of oxygen during charge/discharge processes. Therefore, alternative cathode materials are in urgent demand for better energy storage options. In this regard, phosphate-based polyanionic compounds $LiMPO_4$ [5], $Li_3M_2(PO_4)_3$ [6, 7], $LiVOPO_4F$ [8, 9], and $LiVOPO_4$ [10–12] have gained great interest as alternative cathode materials to the transition metal oxides for lithium-ion battery applications because of their comparable energy density and high electrochemical and thermal stability [13]. These exhibit exceptional stability even under abnormal conditions due to the robust 3D framework of PO_4 polyanion, comprised of robust P-O covalent bonds, which suppress oxygen release during battery cycling [14, 15].

Among them, $Li_3V_2(PO_4)_3$ and $LiVOPO_4$ have gained tremendous interest as next-generation cathode materials due to their multielectron behavior, high operating potentials, higher capacities, and comparable energy density as well as high electrochemical and thermal stability [16–18]. The monoclinic $Li_3V_2(PO_4)_3$ offers the advantages of outstanding thermal stability, high operating voltage, relatively large reversible capacities, and fast ionic mobilities even at low temperatures [19–22]. The triclinic $LiVOPO_4$ offers the advantages of relatively higher working potential (4.0 V versus Li/Li^+) and a capacity of 166 mAh g^{-1} compared to olivine $LiFePO_4$, which despite its higher theoretical capacity of 170 mAh g^{-1}, delivers lower energy density due to its lower operating voltage of 3.45 V [23, 24]. So, these multielectron reaction materials can induce even higher specific capacities regarding transition metal redox reactions with high valence states to deliver the capacities for $Li_3V_2(PO_4)_3$ and $LiVOPO_4$ cathodes of 197 mAh g^{-1} (with redox couples of V^{4+}/V^{3+} and V^{5+}/V^{4+}) and 300 mAh g^{-1} (with redox couples of V^{4+}/V^{5+} and V^{3+}/V^{4+}), respectively [18, 25–28]. However, these phosphate-based cathode materials suffer from the intrinsic problem of low electronic conductivity.

Inspired by B. Kang's off-stoichiometric idea [2], Sun et al. adopted the high energy ball-milling (HEBM) technique on $Li_{2.7}V_{2.1}(PO_4)_3$ to prepare core–shell structure with extra vanadium residing in the external shell. The phase of the external shell was $LiVOPO_4$, which offered extra space for the lithium storage and accommodated extra Li-ions even at high-rate charge and discharge processes. Together with the advantages of small particle sizes and the high electronic conductivity, the cathode delivered a high reversible capacity of 131.5 mAh g^{-1} at the rate of 0.5 C (close to the theoretical capacity); also, the high-rate capacity was considerably improved along with long cycling stability[29]. Therefore, it is expected that the $Li_3V_2(PO_4)_3$ and $LiVOPO_4$ combination may enhance the ionic/electronic conductivities of the composite cathode and improve its electrochemical performance as well [30–33]. Nguyen et al. investigated the structural transformation of $LiVOPO_4$ to $Li_3V_2(PO_4)_3$ with graphene nanofiber (GNF) addition by a solid-state ball-milling method, and resulting cathode materials were found to depict improved capacity and cycling stability [34]. Besides, Kuo et al. reported the structural conversion of triclinic $LiVOPO_4$ to monoclinic $Li_3V_2(PO_4)_3$ at high calcination temperatures (700–800 °C under a reducing atmosphere) led to enhanced capacity [35].

In this regard, two-phase material was prepared by employing the vanadium-excess (V-excess) off-stoichiometric technique. The feasibility of the existence of vanadium in various oxidation states and polymorphs help vanadium phosphates attractiveness for rechargeable Li-ion batteries. We have developed the method by modifying the Li deficiency and V-excess in $Li_3V_{2+x}(PO_4)_3$ in a fixed ratio 3:3 of Li and V. In a recent study, Liu et al. engineered lithium deficiencies in Li-rich layered oxide and demonstrated improved stability and enhanced performance, as Li-deficient cathode acted as a prototype for further performance enhancement due to plenty of vacancies [31, 32, 36]. The strategy we applied by tuning lithium deficiency and vanadium excess was to keep the balance of the chemical valence state, thereby improving the bulk properties as well. This controlled off-stoichiometry in $Li_3V_{2+x}(PO_4)_3$ has been demonstrated to make two-phase composite cathode material LVP-LVOP/C, which helped improve the electrochemical performance with enhanced capacity and obtain stable long cycle life as it accelerates the Li-ion diffusion in the particle and improves electronic conductivity. Furthermore, the sol–gel preparation method offers the advantages of special morphologies, small particle sizes, and large-scale industrial applications due to its simplicity and homogenous mixing of particles at the very atomic level compared to the solid-state method, where homogenous mixing is difficult giving rise to impurity phases. These special morphologies include one-dimensional nanostructures such as nanorods, which effectively improve the electronic conductivity and enhance the electrochemical performance due to high exposed surface area, fast electron transport channels, and facile stress relaxation during charge/discharge processes [37, 38]. In our study, this nanorod-type morphology for the synthesized LVP-LVOP/C composite cathode material for LIBs via a feasible sol–gel preparation method with citric acid used as a reducing agent as well as carbon source showed improved conductivity and electrochemical performance. Such design has been demonstrated to combine the advantages of both $Li_3V_2(PO_4)_3$ and $LiVOPO_4$, to effectively improve capacity, electronic/ionic conductivities, and structural integrity as well. The composite LVP-LVOP/C sintered at 800 °C showed the best performance with the highest initial discharge capacity of 140 mAh g^{-1} at 0.2 C higher than the theoretical value of capacity (133 mAh g^{-1}) in the range of 2.8–4.3 V, high-rate capacity of 82 mAh g^{-1} even at 10 C, and outstanding cycling performance after 1000 cycles at 1 C rate, demonstrating that it is a promising cathode material for LIBs. Meanwhile, the robust structural framework of phosphate units assists facile ion intercalation/de-intercalation versus Li and high stability even after 1000 cycles.

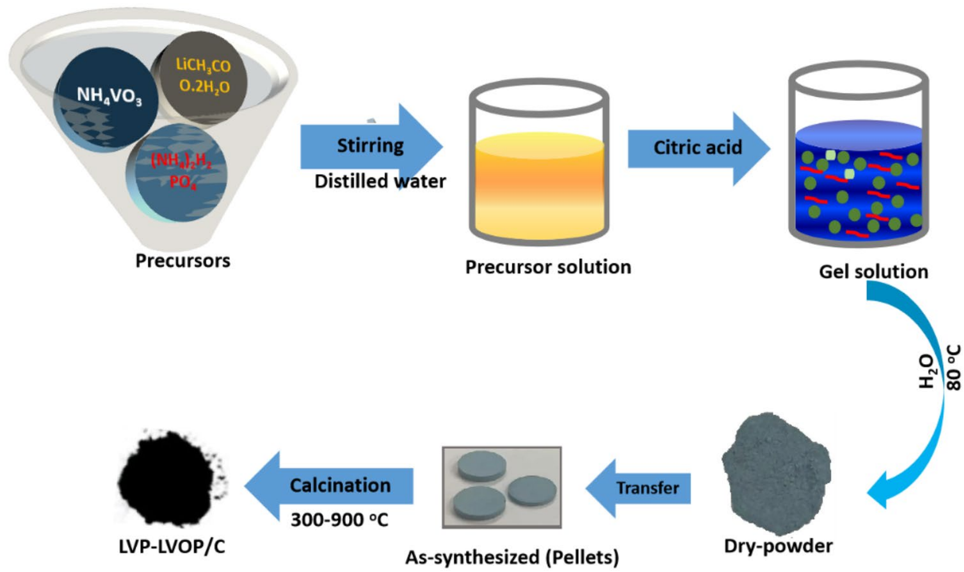

Fig. 1 Schematic of sol–gel synthesis route for LVP-LVOP/C materials

Experimental method

In the present study, we employed sol–gel synthesis as an effective way to get a high-performance LVP-LVOP/C composite. To prepare vanadium-excess sample 0.04 mol of NH_4VO_3, $(NH_4)_2H_2PO_4$ and $LiCH_3COO.2H_2O$ were dissolved in 500 mL of distilled water under constant magnetic stirring at 80 °C. After 2 h citric acid was added, the molar ratios of Li:V:P:$C_6H_8O_7.H_2O$ were (3.1:3:3:3), respectively. Then, the solution was continuously stirred and evaporated on a hot plate for 12 h, forming a gel, which was further dried in an air oven at 60 °C overnight. The obtained precursors were heated in an argon atmosphere at the desired temperatures of 300 °C to 900 °C for 8 h at a 2 °C/min heating rate. For comparison, a pure phase sample was prepared (denoted as LVP/C-750 (pure)) with molar ratios of Li:V:P:$C_6H_8O_7.H_2O$ (3.1:2:3:3) by the same procedure and sintered at 750 °C under argon. The obtained powders were used to prepare the slurry with a ratio of 8:1:1 (active material:SP:PVDF). The schematic diagram of the complete synthesis route is illustrated in Fig. 1 below.

Results and discussion

Figure 2a shows the comparison of X-ray diffraction (XRD) patterns of pure phase LVP/C-750 and V-excess LVP-LVOP/C composite. The diffraction peaks of LVP/C-750 (pure) can be indexed to single-phase crystalline

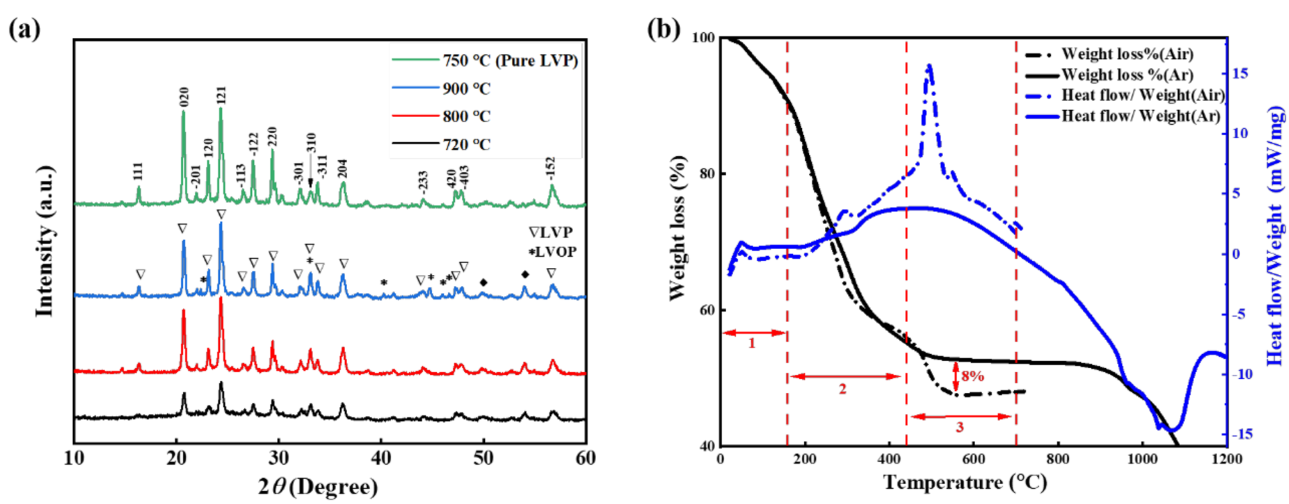

Fig. 2 (**a**) XRD patterns of LVP-LVOP/C powder samples heated at 720 °C, 800 °C, 900 °C and pure phase sample (LVP/C-750 °C) (**b**) TGA and DTA curves of the (V-excess) as-synthesized sample in both air and argon atmosphere

Table 1 Relative proportion of each phase in the composite LVP-LVOP/C

Mass content (%)			
Sample (LVP-LVOP/C)	$Li_3V_2(PO_4)_3$	$LiVOPO_4$	V_2O_3
800 °C	87.3%	7.7%	~5%
900 °C	86.0%	9.0%	~5%

monoclinic $Li_3V_2(PO_4)_3$ (P21/n, JCPDS No. 01–072-7074). However, the XRD patterns of LVP-LVOP/C composites illustrate the growth of a highly crystalline phase. The as-synthesized and low sintering temperature samples are a mixture of Li_3PO_4 and an amorphous phase, which can be regarded as vanadium phosphorous oxide shown in Fig. (S1). Most of the peaks can be indexed to the diffraction patterns of monoclinic $Li_3V_2(PO_4)_3$ phase (P21/n, JCPDS No. 01–072-7074) for the samples prepared (from 720 to 900 °C) under an argon atmosphere. These samples show sharp and intense diffraction peaks positioned at 20.67, 24.36, 47.3, 47.8, and 23.1 with corresponding indices of (020), (121), (420), (403), and (120) ascribed to the existence of $Li_3V_2(PO_4)_3$ as the major phase. With the increase of sintering temperature, the intensities of the characteristic peaks become stronger[39]. However, the XRD pattern shows some low-intensity peaks (marked by the star) that cannot be indexed to $Li_3V_2(PO_4)_3$ phase. These diffraction peaks coincide well with the standard diffraction pattern of the $LiVOPO_4$ phase (P21/n, JCPDS No. 72–2253), illustrating the possible minor phase, which was further confirmed by transmission electron microscope (TEM). Also, there are some peaks of V_2O_3 marked by solid diamond, which was grown due to excess vanadium. So, the samples were characterized to be the monoclinic LVP ($Li_3V_2(PO_4)_3$) as the major phase and triclinic $LiVOPO_4$ as the minor phase and some impurity peaks of V_2O_3. Based on the XRD results, the relative proportion of each phase in the composite LVP-LVOP/C was calculated

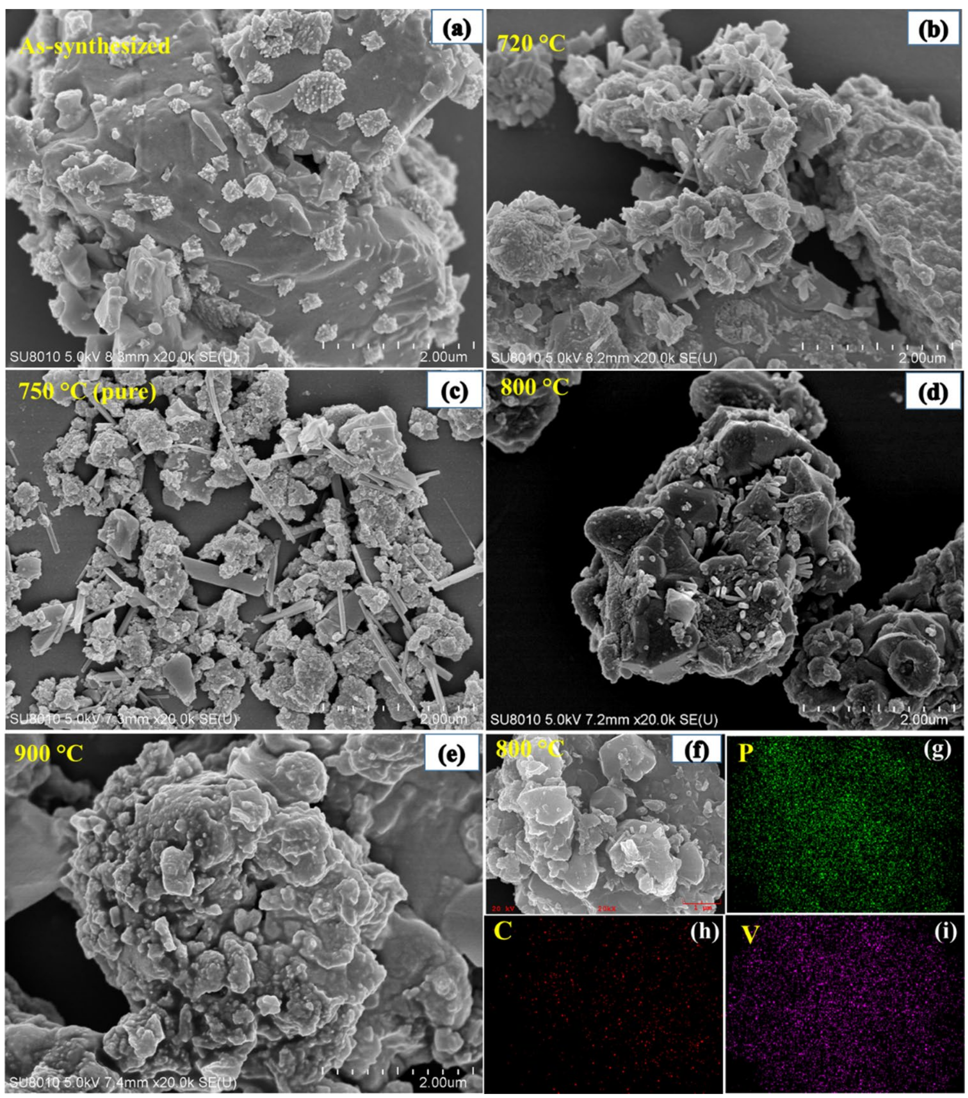

Fig. 3 Surface morphology of LVP-LVOP/C powders sintered at various temperatures. (**a**) As-synthesized, (**b**) 720 °C, (**d**) 800 °C, (**e**) 900 °C, and (**c**) pure phase sample (LVP/C-750 °C) for 8 h. The panel (**f**) shows surface morphology and corresponding (**g**) P, (**h**) C, (**i**) V, EDX elemental mapping of powder sintered at 800 °C

with the WPS module in jade software, and the results are listed in Table 1.

According to the refined phase amounts and their theoretical capacity values (which is 133 mAh g^{-1} for $Li_3V_2(PO_4)_3$ and 166 mAh g^{-1} for $LiVOPO_4$), the theoretical capacity of the composite was calculated by taking the contribution of each phase based on its relative percentage in the composite, which is to be 137 mAh g^{-1}. Also, the carbon content in the composite was not deducted.

TG curves of the (V-excess) as-synthesized sample in the air (dotted line) and argon (solid line) atmosphere are shown in Fig. 2b. It can be divided into three distinct regions. The weight loss is almost the same in the first two regions for both air and argon atmosphere. The initial weight loss with temperatures from 25 to 170 °C should be attributed to the physical and chemical evaporation of water in both air and argon atmosphere. The second stage between temperature 170 and 450 °C with 40% weight loss indicates the pyrolysis of NH_4VO_3, $(NH_4)_2H_2PO_4$, and citric acid within the precursor. It is also represented by the exothermic peak near 300 °C of the DTA curve in the air atmosphere. The third stage is beyond 450 up to 700 °C, and there is 8% extra weight loss in air atmosphere compared to argon atmosphere, corresponding to the emission of CO_2, represented by the exothermic peak near 500 °C in DTA curve of air atmosphere. The sample melts and goes black after heating above a temperature of 700 °C in the air atmosphere [40]. However, the sample heated in argon atmosphere showing the crystallization of $Li_3V_2(PO_4)_3$-$LVOPO_4$ between 600 and 900 °C, and after 900 °C material decomposes. Therefore, based on the above analysis, 720 °C, 800 °C, and 900 °C under argon atmosphere were determined as the sintering temperatures.

The samples were examined by SEM to observe the microstructure of the as-synthesized sample and the samples sintered at 720 to 900 °C in argon. The as-synthesized sample showed that the nanorod-type structure started to grow as shown in Fig. 3a. The nanorod-type surface morphology can be seen clearly for the samples sintered at 720 and 800 °C. However, the crystal is under transition state for sample sintered at 720 °C, as the particles are not fully dispersed, and the interface between the particles is vague as shown in Fig. 3b. However, the nanorod-type particles of size 50–100 nm that are dispersed on the surface of the sample sintered at 800 °C (LVP-LVOP/C-800) can be seen in Fig. 3d. Also, the morphology of secondary particles of size 1–3 μm was irregular for the sample. The significant aggregation occurred between the particles due to the high calcination temperature of 900 °C shown in Fig. 3e, which can be ascribed to the low value of residual carbon content. The length of most of the nanorods for the sample LVP-LVOP/C-800 is about 50–100 nm. These nanorods make the electrical conductivity better and the impedance of samples lower. In contrast, the non-uniform rod-like morphology with length of 0.5–2 μm and thickness of 100–300 nm can be seen for pure phase sample LVP/C-750 C in Fig. 3c. The length and thickness of rods increased due to high ratio of citric acid to vanadium (which is 1.5:1 for LVP/C-750 C and 1:1 for other samples). In order to identify the elemental distribution and composition of LVP-LVOP/C-800, energy

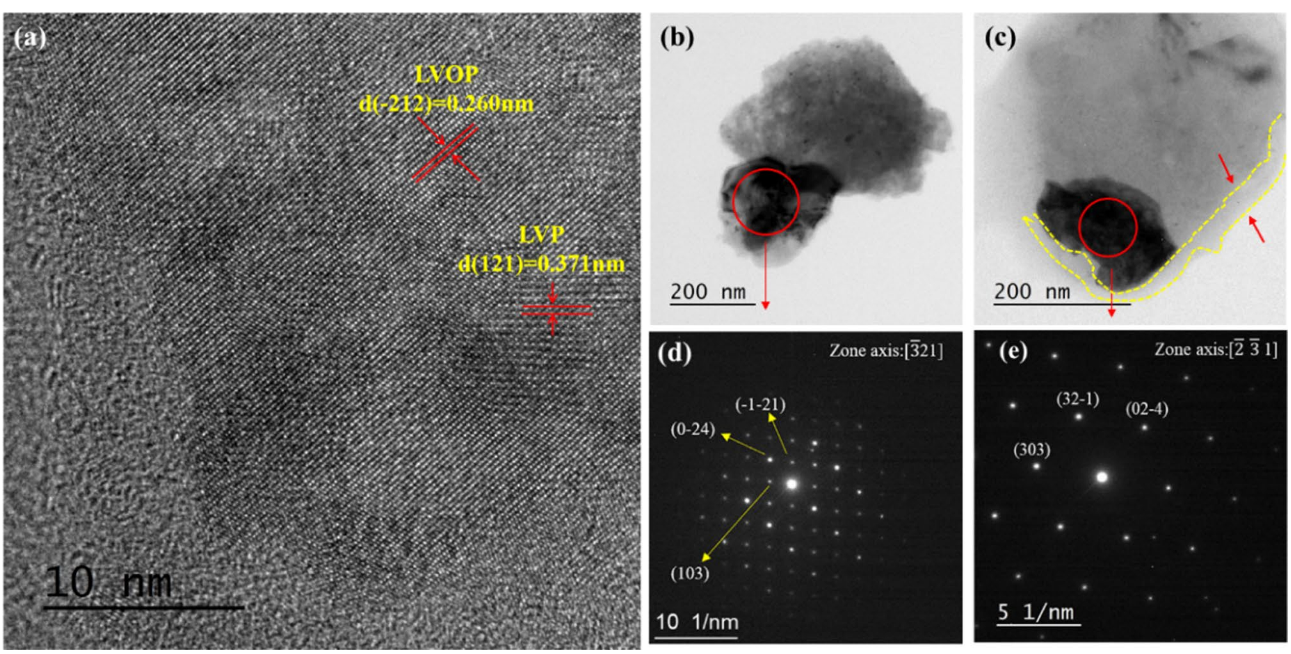

Fig. 4 (**a**) HRTEM surface image; (**d**), (**e**) SAED patterns of area red circled in the image; (**b**), (**c**) LVP–LVOP/C powders sintered at 800 °C

dispersive X-ray spectroscopy (EDX) mapping analysis was performed. The uniform distribution of elements P, C, and V is clearly evident in the sample shown in Fig. 3f–i [39].

Figure 4a shows the HRTEM image of LVP-LVOP/C composite sintered at 800 °C. The two types of lattice fringes corresponding to LVOP and LVP were determined to coexist in the composites. The interplanar spacing of 2.60 Å corresponds to (− 212) lattice planes of triclinic LVOP, and the other d-spacing value of 3.71 Å to the (121) lattice fringes of monoclinic LVP. HRTEM images give us a clear evidence of the coexistence of the two phases, LVOP and LVP, creating a two-phase structure. In the SAED patterns shown in Fig. 4d, e, of area red circled in Fig. 4b, c of the powders, the d-spacing values were found to match the planes of monoclinic $Li_3V_2(PO_4)_3$ confirming the major phase. The carbon layer derived from citric acid, indicated by yellow dotted line as shown in Fig. 4c, is uniformly coated on the surface of the material in the order of nanometer range.

Since XPS is the surface-sensitive technique and it can penetrate only into a depth of around 5 nm, the information of the surface elements is mainly revealed by XPS. The type of surface carbon was analyzed by XPS. In Fig. 5a, b, the peaks at 284.6, and 285.8 eV were assigned to the sp^3 carbon (C–C), and C–O/C = O bonds for the samples LVP-LVOP/C-800 and pure phase LVP/C-750, respectively. The presence of the small carboxyl group (–O–C = O) peak at 288.5 eV describes the incomplete decomposition of citric acid. The valence states of the vanadium for the samples LVP-LVOP/C-800 and pure phase LVP/C-750 were also analyzed by the XPS test; the results are also shown in Fig. 5c, d below. The results reveal that the valence states of V in the external surface area of the sample are + 4 and + 3, respectively. Also, the sample with excess vanadium showed slight decrease in V2p binding energy of vanadium compared to V2p binding energy in pure phase sample.

Figure 6a compares the initial charge and discharge curves for the LVP-LVOP/C and pure phase LVP/C-750 cathode materials in the range of 2.8 to 4.3 V. Three plateaus observed during the charging process at 3.61, 3.70,

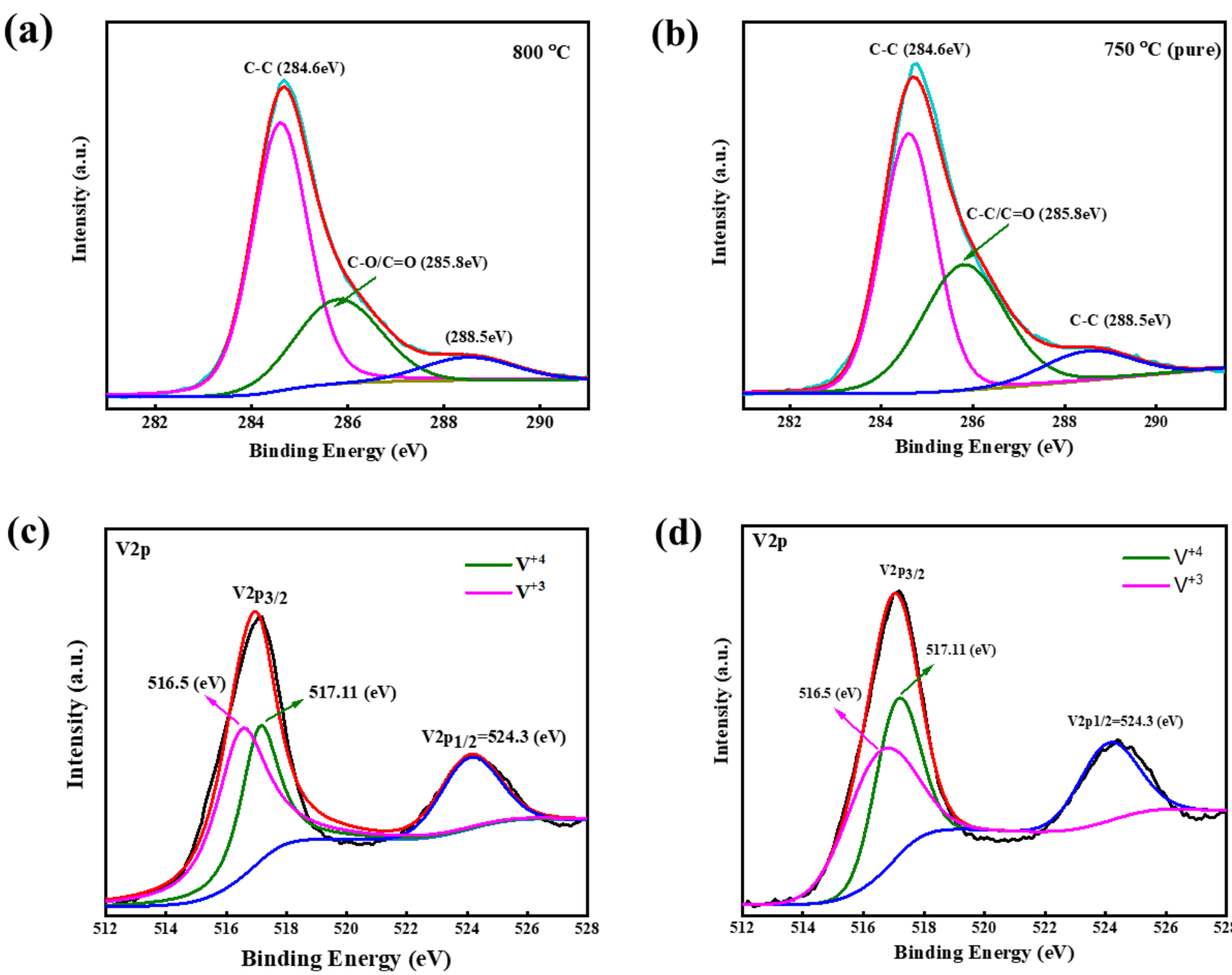

Fig. 5 C1s and V2p XPS spectra and fitting results at (**a**) 800 °C (**b**) 750 °C (pure) and (**c**) 800 °C (**d**) 750 °C(pure), respectively

and 4.10 V, corresponding to the extraction of lithium ions from the cathode. Plateaus appearing during discharge at 4.05, 3.65, and 3.57 represent the insertion of lithium ions in the cathode. The LVP-LVOP/C-800 showed the highest discharge capacity of 140 mAh g^{-1} at 0.2 C, higher than 720 °C, 900 °C, and the pure phase LVP/C-750 powders. The sample sintered at 900 °C showed the lowest discharge capacity due to serious aggregation of particles to form large composite particles resulting in long diffusion paths for Li-ions and insufficient carbon content, which negatively affects the electrochemical performance by inhibiting the intercalation and de-intercalation of Li-ions. Figure 6b shows the cycling performance of the four samples at 0.5 C for 100 cycles. It is important to note that the 100-cycle stability of the LVP/C-800 material was the best. This best performance can be explained by the fact that, at lower temperature, crystallinity was not good, and the material was not fully dispersed. However, with the increase in temperature, the crystallinity increased and dispersion improved, and the two factors reached a balance and the LVP-LVOP/C-800 material exhibited the best cycling stability. With further increase in temperature though the crystallinity of the sample increased, residual carbon content decreased which affected the conductivity negatively for the sample sintered at 900 °C. EIS results for the LVP-LVOP/C and LVP/C-750 batteries are shown in Fig. 6c. The diameter of the semicircle of 720 °C and 800 °C is relatively smaller which corresponds to significantly small charge transfer resistance (Rct) of LVP-LVOP/C to pure phase sample LVP/C-750. Though the sample sintered at 720 °C shows the lowest value of Rct ≈ 120 Ω due to small particle size and relatively higher carbon content. However, the sample lacks in electrochemical performance compared to LVP-LVOP/C-800 (Rct ≈ 200 Ω), which might be due to low crystallinity, poor ionic mobility, and low stability as the material is under transition state. The LVP-LVOP/C-800 has higher ionic mobility and a larger

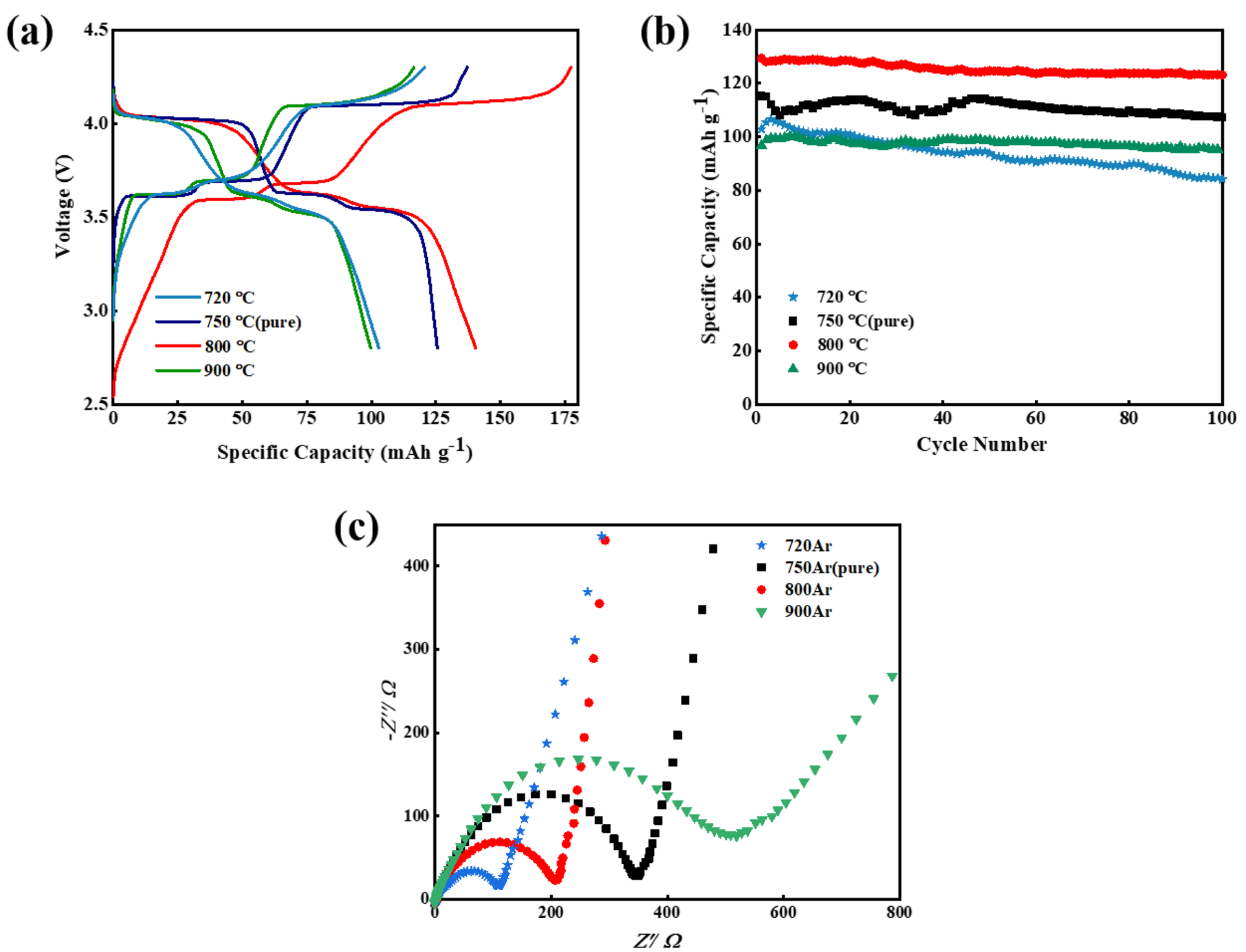

Fig. 6 Comparison of initial charge and discharge curves at 0.2 C (**a**) cycle performance, (**b**) at 0.5 C, and (**c**) Nyquist plots of the LVP-LVOP/C and pure phase LVP/C-750 composite materials

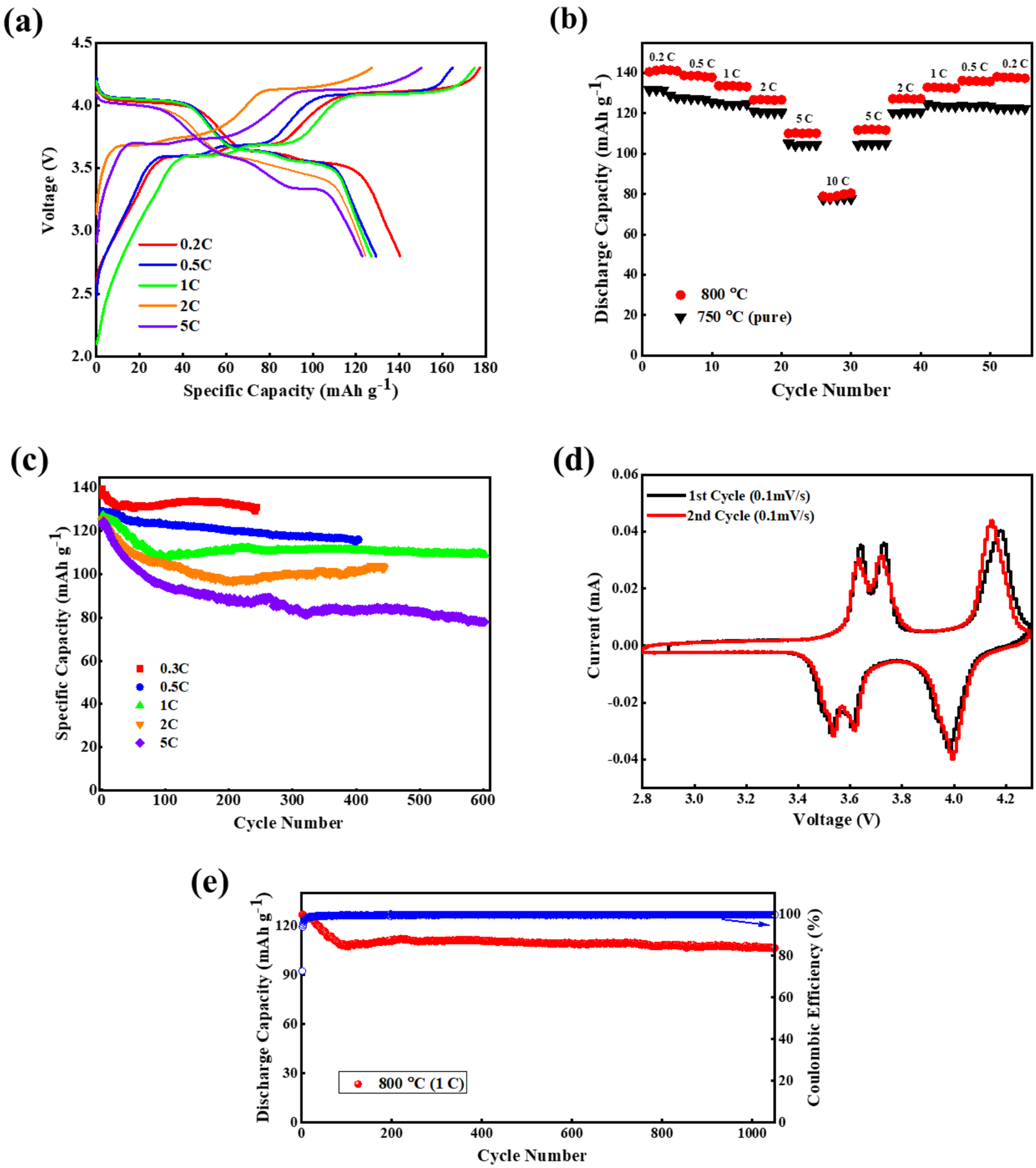

Fig. 7 Initial charge/discharge curves at 0.2 C, 0.5 C, 1 C, 2 C, 5 C of LVP-LVOP/C-800 (**a**) comparison of rate capabilities of sample LVP-LVOP/C-800 with pure sample LVP/C-750 under different discharge rates (**b**) cycle performance; (**c**) at 0.3 C, 0.5 C, 1 C, 2 C; (**d**) cyclic voltammetry curves of LVP-LVOP/C-800 °C composite for two cycles (**e**) its Coulombic efficiency, and cycling stability after 1050 cycles with 85% capacity retention at 1 C

active surface area which lowers the resistance between the interfaces and promotes the diffusion of lithium-ions, thus reduce the charge transfer resistance and improve the exchange current density.

Figure 7a shows the first cycle charge/discharge profiles of LVP-LVOP/C-800 cathode material at various current densities from 0.2 to 5 C (where 1 C = 133.0 mAh g^{-1}) in the voltage range of 2.8–4.3 V. The first cycle profiles exhibit three pairs of charge/discharge plateaus at 3.61/3.57, 3.7/3.65, and 4.10/4.05 V, corresponding to reversible phase conversions during the electrochemical processes. The initial discharge capacity at the rate of 0.2 C is 140 mAh g^{-1} (higher than the theoretical capacity 133.0 mAh g^{-1} for $Li_3V_2(PO_4)_3$. When the current rate is stepwise increased from 0.2 to 10 C, LVP-LVOP/C-800 preserves stable capacities during the entire process shown in (Fig. 7b), thus demonstrating excellent high-rate capability. Figure 7b also shows the comparison of rate capability of LVP-LVOP/C-800 with pure sample LVP/C-750. It can be seen that LVP/C-750 shows reasonable rate performance; however, its specific capacity and cycling stability are relatively poor. The sample LVP-LVOP/C-800 exhibited excellent cycling stability with a capacity retention of 93%, 89%, 85%, 75%, and 65% after 300, 550, 1050, 500, and 650 cycles at discharge rates of 0.3 C, 0.5 C, 1 C, 2 C, and 5 C, respectively, as shown in Fig. 7c. The cyclic voltammetry (CV) technique was performed to further understand the electrochemical insertion/de-insertion processes of Li-ions and determine the reason for the enhanced electrochemical property of sample LVP-LVOP/C-800. Figure 7d shows the CV curve of LVP-LVOP/C-800 at the scan rate of 0.1 mV s^{-1} in the voltage range of 2.8 to 4.3 V (vs. Li/Li^+). The oxidation and reduction peaks seem to appear in such a way that the superimposition of the peaks of $Li_3V_2(PO_4)_3$ and $LiVOPO_4$ materials occurred. Two redox-regions with the average voltages of 3.8 V and 4.1 V correspond to the V^{IV}/V^{III} redox reactions, owing to intercalation and de-intercalation of two Li ions in voltage region 2.8–4.3 V. The small voltage difference in cathodic and anodic peaks corresponds to its excellent electrochemical behavior. The sample exhibited excellent cycling stability with 85% capacity retention after 1050 cycles at the current rate of 1 C and Coulombic efficiency approximately equal to 100% as shown in Fig. 7e.

Conclusions

The V-excess LVP-LVOP/C composite powder samples were successfully synthesized by a combination of non-stoichiometric composition design and simple sol–gel route processing. The XRD results showed the formation of two-phase composite material with $Li_3V_2(PO_4)_3$ and $LiVOPO_4$ as the major and minor phases, respectively, which was further verified by TEM results. The well-dispersed dual-phase LVP-LVOP/C-800 exhibited improved electrochemical performances even higher than pure phase LVP/C-750, which might be ascribed to the synergy between phosphate and oxyphosphate contributing to ionic mobility and enhanced capacity, respectively. The SEM results indicated that nanorod-type morphology was observed for the samples heated at relatively lower sintering temperatures which resulted in low charge transfer resistance and high electronic conductivity. However, with the increase in the sintering temperature, the particle size of the LVP-LVOP/C material continuously increased and the agglomeration of the particles occurred resulting in longer Li-ion diffusion paths. For the sample sintered at an optimized temperature of 800 °C, the best electrochemical property with the highest initial discharge capacity that reached 140 mAh g^{-1} (even higher than the theoretical capacity of $Li_3V_2(PO_4)_3$, 133 mAh/g) in the voltage range of 2.8 to 4.3 V and capacity retention of 93% (with 130 mAh g^{-1} discharge capacity) after 300 cycles were achieved. In addition, the excellent cycling stability with a capacity retention of 85% at a high discharge rate of 1 C after 1050 cycles was retained. Hence, the controlled non-stoichiometry with excess vanadium has been demonstrated to improve the electrochemical performance with enhanced capacity due to the contribution of $LiVOPO_4$ to the capacity. The excess vanadium has been confirmed to locate in the composite to form the $LiVOPO_4$ phase and can accommodate more Li^+ ions by offering more vacancies for Li storage during the charge/discharge processes. Together with low charge transfer resistance, special morphology, and improved electronic and ionic conductivity, the V-excess dual-phase composite LVP-LVOP/C-800 has shown much improved electrochemical performance and can serve as an outstanding candidate to be applied to high power applications.

Supplementary information The online version contains supplementary material available at https://doi.org/10.1007/s10008-021-04986-y.

Funding This research is financially supported by Anhui Natural Science Foundation (No. 1908085ME151, KJ2020A0263), China Postdoctoral Science Foundation (No. 2020M673404), Anhui province high-end talent grant (DT18100044), the national level foreign expert introduction plan project (G20190219004), and by National Natural Science Foundation of China through Grant No. 51802322.

Declarations

Conflict of interest The authors declare no competing interests.

References

1. Xu X, Xiong F, Meng J et al (2020) Vanadium-based nanomaterials: a promising family for emerging metal-ion batteries. Adv Funct Mater 30:1–36. https://doi.org/10.1002/adfm.201904398
2. Kang B, Ceder G (2009) Battery materials for ultrafast charging and discharging. Nature 458:190–193. https://doi.org/10.1038/nature07853
3. Nojima A, Sano A, Kitamura H, Okada S (2019) Electrochemical characterization, structural evolution, and thermal stability of livopo4 over multiple lithium intercalations. Evergreen 6:267–274. https://doi.org/10.5109/2547346

4. Cai Z, Ma Y, Huang X et al (2020) High electrochemical stability Al-doped spinel LiMn2O4 cathode material for Li-ion batteries J Energy Storage 27. https://doi.org/10.1016/j.est.2019.101036
5. Chung S-Y, Bloking JT, Chiang Y-M (2002) Electronically conductive phospho-olivines as lithium storage electrodes. Nat Mater 1:123–128. https://doi.org/10.1038/nmat732
6. Li Y, Zhou Z, Ren M et al (2006) Electrochemical performance of nanocrystalline Li3V2(PO4)3/carbon composite material synthesized by a novel sol–gel method. Electrochim Acta 51:6498–6502. https://doi.org/10.1016/j.electacta.2006.04.036
7. Wang Y, Tang Y, Zhong B et al (2014) Facile synthesis of Li3V2(Po4) 3/C nano-flakes with high-rate performance as cathode material for Li-ion battery. J Solid State Electrochem 18:215–221. https://doi.org/10.1007/s10008-013-2249-2
8. Barker J, Gover RKB, Burns P, Bryan A (2005) A symmetrical lithium-ion cell based on lithium vanadium fluorophosphate, LiVPO4F. Electrochem Solid-State Lett 8:285–288. https://doi.org/10.1149/1.1897352
9. Kim M, Lee S, Kang B (2017) High energy density polyanion electrode material: LiVPO4O1-xFx (x ≈ 0.25) with Tavorite Structure. Chem Mater 29:4690–4699. https://doi.org/10.1021/acs.chemmater.7b00124
10. Ren MM, Zhou Z, Gao XP et al (2008) LiVOPO4 hollow microspheres: one-pot hydrothermal synthesis with reactants as self-sacrifice templates and lithium intercalation performances. J Phys Chem C 112:13043–13046. https://doi.org/10.1021/jp804335b
11. Zheng JC, Han YD, Zhang B et al (2014) Comparative investigation of microporous and nanosheet LiVOPO4as cathode materials for lithium-ion batteries. RSC Adv 4:41076–41080. https://doi.org/10.1039/c4ra06797e
12. He G, Bridges CA, Manthiram A (2015) Crystal chemistry of electrochemically and chemically lithiated layered αI-LiVOPO4. Chem Mater 27:6699–6707. https://doi.org/10.1021/acs.chemmater.5b02609
13. Shen C, Zhang B, Zheng JC et al (2015) Effect of sintering time on the synthesize of the multi-layered core-shell LiVOPO4-Li3V2(PO4)3 composite for Li-ion batteries. J Alloys Compd 622:771–776. https://doi.org/10.1016/j.jallcom.2014.10.198
14. El-Desoky MM, Al-Syadi AM, Al-Assiri MS et al (2016) Electrochemical performance of novel Li3V2(PO4)3 glass-ceramic nanocomposites as electrodes for energy storage devices. J Solid State Electrochem 20:2663–2671. https://doi.org/10.1007/s10008-016-3267-7
15. Thanh L, Huynh N, Thuy T et al (2018) Carbon-coated LiFePO 4 – carbon nanotube electrodes for high-rate Li-ion battery. 2247–2254
16. Quackenbush NF, Wangoh L, Scanlon DO et al (2015) Interfacial effects in ε-LixVOPO4 and evolution of the electronic structure. Chem Mater 27:8211–8219. https://doi.org/10.1021/acs.chemmater.5b02145
17. Kim M, Avdeev M, Kang B (2020) Multielectron-capable Li-rich polyanion material with high operating voltage: Li5V2PO4F8 for Li-ion batteries. ACS Energy Lett 5:403–410. https://doi.org/10.1021/acsenergylett.9b02451
18. Whittingham MS, Siu C, Ding J (2018) Can multielectron intercalation reactions be the basis of next generation batteries? Acc Chem Res 51:258–264. https://doi.org/10.1021/acs.accounts.7b00527
19. Tai LH, Zhao Q, Sun LQ et al (2015) A study of the electrochemical behavior at low temperature of the Li3V2(PO4)3 cathode material for Li-ion batteries. New J Chem 39:9617–9626. https://doi.org/10.1039/c5nj01895a
20. Huo H, Lin Z, Wu D et al (2019) Investigating the structure of an active material-carbon interface in the monoclinic Li3V2(PO4)3/C composite cathode. ACS Appl Energy Mater 2:3692–3702. https://doi.org/10.1021/acsaem.9b00410
21. Membreño N, Park K, Goodenough JB, Stevenson KJ (2015) Electrode/electrolyte interface of composite α-Li3V2(PO4)3 cathodes in a nonaqueous electrolyte for lithium ion batteries and the role of the carbon additive. Chem Mater 27:3332–3340. https://doi.org/10.1021/acs.chemmater.5b00447
22. Ahmani Ferdi C, Belaiche M, Iffer E (2021) Structural, electrochemical, electronic, and magnetic properties of monoclinic LixV2(PO4)3 for x = 3, 2, 1 using first-principles calculations. J Solid State Electrochem 25:301–313. https://doi.org/10.1007/s10008-020-04808-7
23. Nojima A, Sano A, Fujita S et al (2019) Evaluation of α 1-LiVOPO 4, β-LiVOPO 4, and α-LiVOPO 4 synthesized from a same precursor by hydrothermal method. J Electrochem Soc 166:A3731–A3738. https://doi.org/10.1149/2.0691915jes
24. Li X, Shao Z, Liu K et al (2018) Effect of F-doping on the properties of LiFePO4-x/3Fx/C cathode materials via wet mechanical agitation-assisted high-temperature ball milling method. J Solid State Electrochem 22:2837–2843. https://doi.org/10.1007/s10008-018-4001-4
25. Shi Y, Zhou H, Britto S et al (2019) A high-performance solid-state synthesized LiVOPO4 for lithium-ion batteries. Electrochem commun 105:106491 https://doi.org/10.1016/j.elecom.2019.106491
26. Shi HY, Jia Z, Wu W et al (2020) The development of vanadyl phosphate cathode materials for energy storage systems: a review. Chem - A Eur J 26:8190–8204. https://doi.org/10.1002/chem.201905706
27. Lin YC, Hidalgo MFV, Chu IH et al (2017) Comparison of the polymorphs of VOPO4 as multi-electron cathodes for rechargeable alkali-ion batteries. J Mater Chem A 5:17421–17431. https://doi.org/10.1039/c7ta04558a
28. He G, Kan WH, Manthiram A (2018) Delithiation/lithiation behaviors of three polymorphs of LiVOPO 4. Chem Commun 54:13224–13227. https://doi.org/10.1039/C8CC07446A
29. Sun P, Wang X, Zhu K et al (2017) Core-shell-structured Li3V2(PO4)3-LiVOPO4 nanocomposites cathode for high-rate and long-life lithium-ion batteries. RSC Adv 7:3101–3107. https://doi.org/10.1039/c6ra26790d
30. Sun P, Su N, Wang Y et al (2017) Synthesizing nonstoichiometric Li3-3:XV2+x(PO4)3/C as cathode materials for high-performance lithium-ion batteries by solid state reaction. RSC Adv 7:32721–32726. https://doi.org/10.1039/c7ra04842d
31. Sun P, Qin S, Wang X et al (2015) Off-stoichiometric Li3-3xV2+x(PO4)3/C as cathode materials for high-performance lithium-ion batteries. J Power Sources 293:922–928. https://doi.org/10.1016/j.jpowsour.2015.06.027
32. Zhang B, Shen C, Zheng J et al (2014) Synthesis and characterization of a multi-layer core-shell composite cathode material LiVOPO 4 -Li 3 V 2 (PO 4) 3. J Electrochem Soc 161:A748–A752. https://doi.org/10.1149/2.050405jes
33. Zhong S, Zhang X, Liu J, Sui Y (2020) Study on xLiVPO4F·yLi3V2(PO4)3/C composite for high-performance cathode material for lithium-ion Batteries. Front Chem 8:1–9. https://doi.org/10.3389/fchem.2020.00361
34. Nguyen VH, Wang WL, Gu HB (2015) Enhanced electrochemical performance of Li3V2(PO4)3 structurally converted from LiVOPO4 by graphite nanofiber addition. Ceram Int 41:5403–5413. https://doi.org/10.1016/j.ceramint.2014.12.105
35. Kuo HT, Bagkar NC, Liu RS et al (2008) Structural transformation of LiVOPO4 to Li3v 2(PO4)3 with enhanced capacity. J Phys Chem B 112:11250–11257. https://doi.org/10.1021/jp803210w
36. Liu P, Zhang H, He W et al (2019) Lithium deficiencies engineering in Li-rich layered oxide Li1.098Mn0.533Ni0.113Co0.138O2 for high-stability cathode. J Am Chem Soc 141:10876–10882. https://doi.org/10.1021/jacs.9b04974

37. Kuganathan N, Chroneos A (2019) Defects and dopant properties of Li3V2(PO4)3. Sci Rep 9:1–8. https://doi.org/10.1038/s41598-018-36398-w
38. Huang C, Chen D, Huang Y, Guo Y (2013) Sol-gel synthesis of Li3V2(PO4) 3/C cathode materials with high electrical conductivity. Electrochim Acta 100:1–9. https://doi.org/10.1016/j.electacta.2013.03.073
39. Ni Q, Bai Y, Yang Z et al (2017) Wet-chemical coordination synthesized Li3V2(PO4)3/C for Li-ion battery cathodes. J Alloys Compd 729:49–56. https://doi.org/10.1016/j.jallcom.2017.09.106
40. Zhou H, Shi Y, Xin F et al (2017) ϵ- and β-LiVOPO4: phase transformation and electrochemistry. ACS Appl Mater Interfaces 9:28537–28541. https://doi.org/10.1021/acsami.7b07895